Journal of Power Sources 396 (2018) 621–631

Contents lists available at ScienceDirect

Journal of Power Sources

journal homepage: www.elsevier.com/locate/jpowsour

# Comparative study of various cathodes for lithium ion batteries using an enhanced Peukert capacity model

Ryan O'Malley, Lin Liu, Christopher Depcik*

*University of Kansas, Department of Mechanical Engineering, 3138 Learned Hall, 1530 W. 15th Street, 66045-4709, Lawrence, KS, USA*

## HIGHLIGHTS

- Enhanced Peukert capacity model for electric vehicles including temperature effects.
- Five different cathodes and two types of crystal structures tested.
- Comparative analysis highlights unique discharge effects for lithium ion cells.
- Model parameters largely follow patterns consistent with chemistry literature.
- Absolute capacity factor improves understanding of remaining energy stored.

## GRAPHICAL ABSTRACT

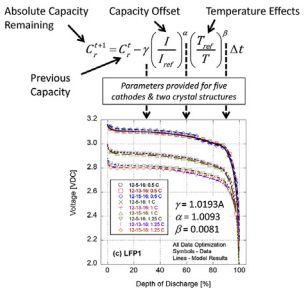


## ARTICLE INFO

*Keywords:*
Lithium ion
Cathode
Numerical model
Temperature effects
State of charge
Optimization

## ABSTRACT

Numerical models for battery management systems must be computationally efficient with enough accuracy for predictive usage when the vehicle is operating. For electric vehicles (EVs), this requires accounting for capacity offset, temperature dependency, and battery aging effects. This effort provides an enhanced formulation of Peukert's equation including temperature effects and the inclusion of an absolute capacity that is calibrated to five different cathodes ($LiCoO_2$, $LiCoNiAlO_2$, $LiNiMnCoO_2$, $LiMnNiO_2$, and $LiFePO_4$) with two types of crystal structures (layered and olivine) from four manufacturers. After data collection using a Vencon battery analyzer and two thermistors measuring self-heating temperature swings, the results demonstrate that the model works relatively well in predicting the State of Charge curve. As expected, the capacity specific parameter is near unity when simulating low offset olivine compounds; whereas, the temperature dependent variable illustrates a wide-range of values with cobalt constituted chemistries on the higher end. Additionally, the model tends to perform better for non-spinel compounds and that manufacturer specified nominal capacities are around 95–99% of the model defined absolute capacity. Overall, the technique of separating current and temperature based phenomena and recognizing modeled patterns that align with current literature are useful steps in developing an efficient battery model.

## 1. Introduction

Investigating the general trend of sales for plug-in Electric Vehicles (EVs) in the United States, after the initial rise from 2010 to 2014, consumer purchases have started to level off [1]. One potential reason that continued growth is not seen is because range anxiety is still an issue [2]. While research is underway for next generation battery technologies with higher energy densities, they are still years away

* Corresponding author.
*E-mail addresses:* ryanomalley13@gmail.com (R. O'Malley), linliu@ku.edu (L. Liu), depcik@ku.edu (C. Depcik).

https://doi.org/10.1016/j.jpowsour.2018.06.066
Received 7 February 2018; Received in revised form 9 June 2018; Accepted 15 June 2018
0378-7753/ 

**Table 1**
Basic parameters of the lithium-ion batteries under study.

| Name | Cathode Chemistry | Crystal Structure | Manufacturer Part Number | Nominal Capacity [Ah] | Nominal Voltage [VDC] | Voltage Range [VDC] | Max Load [A] |
|---|---|---|---|---|---|---|---|
| LCO | $LiCoO_2$ | Layered | LG ICR18650C2 | 2.8 | 3.7 | 3.0–4.3 | 4.0 |
| NCA | $LiCoNiAlO_2$ | Layered | Panasonic NCR18650A | 3.1 | 3.6 | 2.5–4.2 | 6.0 |
| NMC1 | $LiNiMnCoO_2$ | Layered | LG ICR18650B4 | 2.6 | 3.6 | 2.8–4.2 | 5.0 |
| NMC2 | $LiNiMnCoO_2$ | Layered | LG ICR18650S3 | 2.2 | 3.6 | 3.0–4.2 | 3.2 |
| LMN | $LiMnNiO_2$ | Layered | LG LMN18650-2000 | 2.0 | 3.6 | 3.0–4.2 | 2.0 |
| LFP1 | $LiFePO_4$ | Olivine | A123 APR18650M1-A | 1.1 | 3.3 | 2.0–3.6 | 30.0 |
| LFP2 | $LiFePO_4$ | Olivine | A123 IFR18650P120 | 1.2 | 3.2 | 2.0–3.65 | 18.0 |
| LFP3 | $LiFePO_4$ | Olivine | AA LFP-22650-2500-16C | 2.5 | 3.2 | 2.0–3.65 | 12.5 |

from implementation in a commercial vehicle. Therefore, in order to facilitate a greater range with current battery chemistries requires the on board Battery Management System (BMS) to predict the capacity left within a battery pack more accurately. This requires highly efficient models that have low computational cost. In this area, Peukert developed one of the first models for lead-acid batteries through the formulation of his famous equation [3]:

$$C_P = I^k t \tag{1}$$

where $C_P$ is the capacity at 1-A discharge rate in [Ah], $I$ is the current in [A], $k$ is an exponent multiplier, and $t$ is time. The simplicity of its formulation allows for straightforward implementation with little computer processing required and the basic idea is to relate the capacity of the battery to its discharge rate. Specifically, as the discharge rate increases, ohmic losses increase, and ion diffusion/migration in the electrodes cannot catch up with an increasing discharging current resulting in a lower recovery rate and, eventually, a smaller battery capacity. The exponent $k$ (i.e., Peukert's constant) should be near one for a well-performing battery. With respect to lead-acid batteries, often this value is 10%–30% greater than one [4]. When investigating modern lithium-ion batteries, even though high discharge rate currents can lead to side chemical reactions, material phase and structure transitions along with growth of internal cell resistance [5–8], $k$ is found to be close to one [9].

While other options exist for simulating batteries with higher fidelity, like electrochemical equations [10], multi-layer neural networks employing machine learning [11,12], and cell equivalent circuits [13–15], the simplicity of use and uncomplicated calibration of Peukert's equation provides for continued interest if errors with its implementation can be mitigated. Hence, a prior effort involved a reinvention of this equation to account for temperature effects and the inclusion of an absolute capacity [9]. In general, this absolute capacity is designed to remove the relative randomness of nominal capacity (e.g., a 20-hr rate) while also accounting for the fact that batteries undergoing high discharge rates still have capacity remaining when the discharge rate is reduced [16,17]. Moreover, if able to simulate the battery correctly, this absolute capacity allows for potential implementation of battery aging by simply degrading a single factor with vehicle life (e.g., capacity loss for $LiFePO_4$ batteries [18]). An analogy can be drawn to the catalyst modeling field where Oh and Cavendish implemented a single parameter to account for the sintering of precious metals (i.e., catalyst aging) over time [19].

The previous effort illustrated that under changing temperature environments, vehicle size batteries (60–100 A h) were able to be successfully modeled using this updated model [9]. However, that work simulated only a single known chemistry ($LiFePO_4$) using three different battery manufacturers with one unknown chemistry also tested. Therefore, this effort investigates five different cathode materials ($LiCoO_2$, $LiCoNiAlO_2$, $LiNiMnCoO_2$, $LiMnNiO_2$, and $LiFePO_4$) with two types of crystal structures (layered and olivine) for lithium ion batteries from four manufacturers. The battery capacities are between 1.1 and 3.1 A h consisting of experiments ranging from 0.5C to 1.25C. Of note, use of this conventional C-rating based on manufacturer-supplied nominal values allowed for consistency between tests. The following sections first present the experimental setup and methodology employed for data collection along with the revised model. Then, a discussion revolving around the differences between the chemistries tested follows the provided results including optimized model constants.

## 2. Materials and methods

In order to understand how lithium ion cathodic chemical kinetics influences capacity consumption, we selected two types of crystal structures and five cells with different cathode materials. Cost and equipment limiting factors led to the decision to use small 18650 sized batteries that are 18 mm in diameter and 65 mm long and can store 1–4 A h. Table 1 lists the five cells tested along with basic battery specifications and Fig. 1 illustrates the two types of crystal structures employed. Their classification is based on the dimensionality of the $Li^+$ ions transport during de/intercalation, in which $Li^+$ ions are transported through one-dimensional (1-D) (olivine) and two-dimensional (2-D) (layered) compounds. As illustrated in Fig. 1, the olivine compounds, e.g., Li $[M]PO_4$ ($M$ = Fe, Mn), consist of a 1-D channel of $Li^+$ ions transported within a distorted hexagonal closed-packed (HCP) oxygen framework, which contains Li and Fe located in half the octahedral sites and P ions in one-eighth of the tetrahedral sites [20]. In comparison, the layered compounds, e.g., Li $[M]O_2$ ($M$ = Co, Ni), have the oxygen ion close-packed in a cubic arrangement with the transition metal elements and $Li^+$ ions occupying the octahedral sites [21], where the $Li^+$ ions are transported via 2-D planes. The specific cathodes under study are lithium cobalt oxide ($LiCoO_2$), lithium nickel cobalt aluminum oxide ($LiCoNiAlO_2$), lithium nickel magnesium cobalt oxide ($LiNiMnCoO_2$), lithium magnesium nickel oxide ($LiMnNiO_2$), and

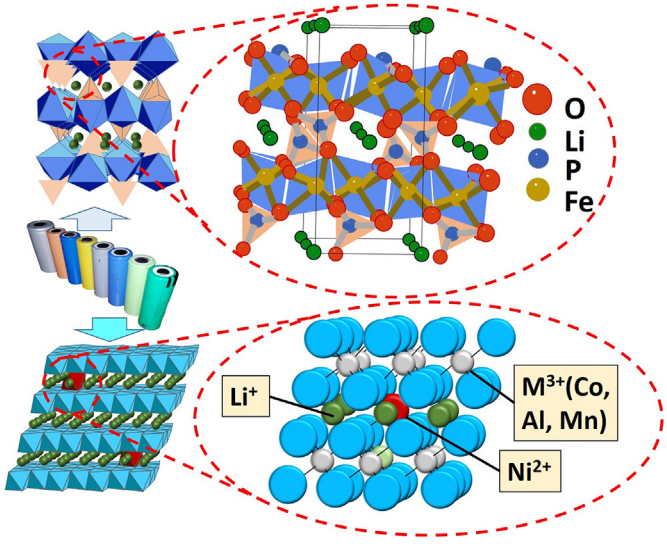


**Fig. 1.** The two types of crystal structures (top: olivine; bottom: layered) employed in this analysis.

lithium iron phosphate ($LiFePO_4$). For convenience, Table 1 refers to them by the following names: LCO, NCA, NMC, LMN, and LFP, respectively.

The choice of these cathodes focuses on the state of the art for EV usage. Specifically, Chevy Volt employs an NMC-LMO ($LiMn_2O_4$) formulation [22] and so do a number of other manufacturers [23]. However, because of the advanced nature of LMN batteries in contrast to the LMO chemistry (e.g., LMN's higher energy density [24]) along with the fact that Nissan Leaf utilizes this distinct chemistry [25], LMN was selected for testing. Of note, analogous research by Dubarry et al. [26] finds that Peukert's equation has been applied to LMO batteries; hence, there does not appear to be a limit to the modeling methodology discussed here for spinel structures. In comparison, Tesla uses the NCA battery chemistry [27]; whereas, LFP is employed for mobile applications in China [28]. Furthermore, the use of LCO helps to understand how the addition of particular species (i.e., cobalt, nickel, aluminum, and manganese) can alter discharge and temperature profiles. In addition, analysis of multiple examples of LFP and NMC types occurred because EV research projects at the authors' university involve these specific chemistries (e.g. [29]).

Data collection used a Vencon (Vencon Technologies Inc., Toronto, Canada) UBA-5 battery analyzer (Fig. 2) that applies graphically developed charging and discharging routines entered via a personal computer to which the UBA-5 then prints the results via a comma separated variable file. The basic idea behind each program is to load the cell to its low cut off voltage and then charge to its maximum safe voltage (i.e., 100% State of Charge (SOC)). After a 1 h rest to achieve equilibrium, application of the desired load happens until the cell reaches the low cut off voltage once again (i.e., 0% SOC). At the end of each test, the Vencon recharges the cells to 30% SOC for safe storage. For this effort, three different loads are applied to a battery with charge events and rests in between to allow for chemistry equalization and the temperature to return to ambient conditions. Moreover, control of each step utilizes specific parameters depending on the battery specification (e.g., maximum C-rating) and test desired.

Although cell temperature is not a controlled variable here, self-heating can affect capacity drain [30]. Hence, two Philips (Philips Electronics N.V., Amsterdam, Netherlands) model SN74LS04 thermistors capture the extent of self-heating for these tests. Consistency between all experiments required using discharge C-Ratings of 0.5, 0.75, 1, and/or potentially 1.25 (if allowed by manufacturer specifications) based on the maximum load information in Table 1. This ensures testing the batteries under relatively similar events even if their nominal capacities are different. For instance, choosing a 1.1 A discharge rate for LFP1 and NCA would result in significantly different C-Ratings (1C and 0.35C, respectively) and potentially dissimilar internal chemistry effects.

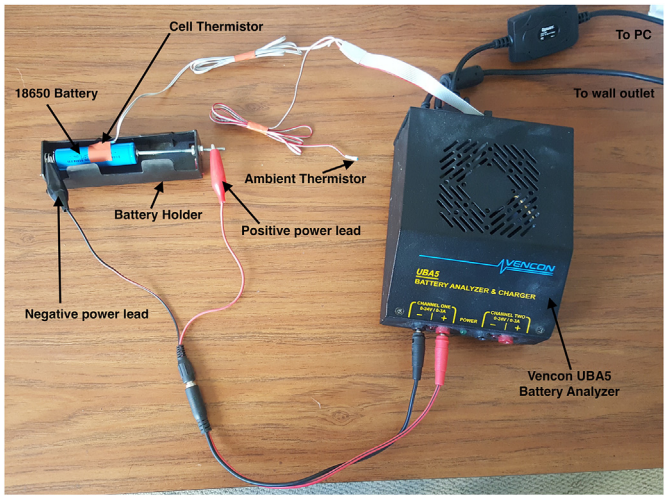


**Fig. 2.** Picture of the experimental setup highlighting the use of the Vencon UBA5 battery analyzer for data collection.

As indicated, experimentation employed the high and low safe voltages in order to test over the entire range of battery capacity. In regards to this concept, Andrea addresses the issue of varying battery capacities during dissimilar discharge events by separating definitions of SOC and Depth of Discharge (DOD) [31]. In specific, SOC is always between 0 and 100% regardless if there is energy in the battery after a discharge event. This value is explicitly defined via voltage points and its rate of change is not computationally definable. However, measuring the DOD in Ah and analyzing the time rate of change of the DOD allows for better control and an understanding of a battery's behavior. Along these lines, rather than rating battery capacity based on a usage time (e.g., 20-hr rate capacity in Table 1), this effort outlines a new definition of absolute capacity. Specifically, a battery will always contain a remaining maximum available capacity ($C_r$) as specified in discrete-time where $t$ represents the discrete-time instant, and $t+1$ differs from $t$ by the time step taken (i.e., $\Delta t$):

$$C_r^{t+1} = C_r^t - \Delta C_r \tag{2}$$

Here, the absolute capacity $C_r^0$ of a fully charged battery is at time equal to zero. The remaining capacity is absolute after a known discharge event and allows for future predictions, regardless of the potential discharge conditions. The last term in the equation is what varies based on the specific environment and use, giving this model its versatility and accuracy. In short, at any one time, the remaining capacity is fixed but the rate it decreases varies as a function of load (i.e., capacity offset) and temperature.

Capacity offset via Peukert's equation is modified here to be non-dimensional via a reference current ($I_{ref}$) of 1 A. Similar to Peukert's constant ($k$) in Eqn. (1), a constant alpha ($\alpha$) impacts the discharge rate:

$$\Delta C_r(I) = \left(\frac{I}{I_{ref}}\right)^{\alpha} \tag{3}$$

Based on Eqn. (3), the conclusion can be drawn that a battery that is unaffected by capacity offset has an exponential value of one.

The more debated property of capacity modeling is the temperature dependency. A brief understanding of chemistry demonstrates the significance of the kinetic parameters that govern a reaction's behavior. These include, but are not limited to, temperature, pressure, and energy input and can affect the kinetic reaction and diffusion occurring simultaneously inside batteries [32,33]. More importantly, the degradation of battery is not only location-dependent but temperature-dependent [34,35]. This elucidates the idea that inclusion of temperature-based effects is crucial when investigating batteries. Our previous studies acknowledge this need; however, the exact relationship is unclear [16,36]. Both thermal energy conservation and Arrhenius equations can describe the changes of battery temperature and temperature-dependent physicochemical properties; however, they are generally numerically expensive. Previous experimental verification has expressed that capacity drain rate increases as the cell temperature decreases (cold temperature increases the internal resistance), inversely to amperage [9]:

$$\Delta C_r(T) = \left(\frac{T_{ref}}{T}\right)^{\beta} \tag{4}$$

where the term is made dimensionless by scaling it by a reference temperature ($T_{ref}$) of 298 K. The exponential constant ($\beta$) is analogous to $\alpha$ in Eqn. (3) and drives the temperature relationship. Due to the common use of graphite as an anode, the temperature effects in large automotive lithium-ion batteries vary mainly based on their cathode and electrolyte materials. This can largely outweigh the load offset or it can be nearly negligible with experimental ranges for $\beta$ values between 0.3 and 3.0 [9].

Tying the two dimensionless relationships to the discharge rate simply requires one more term. From Eqn. (2), the instantaneous discharge rate ($\Delta C_r$) is measured as capacity in amp-hours; therefore, its magnitude must be scaled by a constant presented by γ:

$$\Delta C_r = \gamma\left(\frac{I}{I_{ref}}\right)^{\alpha}\left(\frac{T_{ref}}{T}\right)^{\beta}\Delta t \tag{5}$$

The choice of combining the two factors of Eqn. (3) and Eqn. (4) into Eqn. (5) through multiplication stemmed from the fact that both current and temperature influence capacity offset in a similar manner. As current increases and temperature decreases, capacity offset grows. It is assumed that these effects are multiplicative rather than additive because of the exponential impact of temperature on chemical reaction rates [37]. Generally, under C-Ratings that are representative of EV usage (e.g., 1C [38]), capacity offset and self-heating are intrinsically linked. Even when employing extremely high convective cooling rates in order to attempt to maintain a singular temperature for testing, there still could be a temperature difference between center and surface temperatures [39]. Therefore, the choice was made to compare the levels of self-heating based on chemistry while using the multiplication dependency in Eqn. (5) for modeling purposes. Future work can endeavor to isolate these effects using temperature-controlled chambers. In addition, this multiplicative option prevents the inclusion of another constant to calibrate helping to reduce the possibility of local minimums during optimization.

Prior usage of Eqn. (5) wrapped the time term ($\Delta t$) into the scaling term (γ) [9], yielding its units as Ah. This suffices to balance the relationship physically; however, it becomes problematic when using the equation elsewhere. While applying past knowledge to a new form of testing, the authors found benefit in separating out the time term resulting in Eqn. (5) helping to illustrate perfect battery characteristics; i.e., $\alpha$ and γ equal to one with $\beta$ equal to zero. Hence, a 100 A h perfect battery discharged at 5 A will result in a $\Delta t$ equal to 20 h. Therefore, the parameters of Eqn. (5) illustrate the deviation away from ideal attributes. The inclusion of units on γ (amps) is simply a matter of balancing the units of this equation to allow for relative comparison of batteries. In particular, γ now has a consistent unit for comparison since following Peukert's equation would result in units of amps$^{1-\alpha}$. In a perfect scenario, the nominal rating supplied by the battery manufacturer would equal the absolute capacity, $C_r^0$. This absolute capacity is the point at which a BMS will define as 100% SOC and Eqn. (5) illustrates how software will decrease this value during operation. The use of this model requires data collection over many test conditions and iterations giving rise to calibration of the four parameters: $\alpha$, $\beta$, γ, and $C_r^0$. However, once known for a given battery chemistry, the BMS can accurately rely on the SOC value in a multitude of driving conditions.

Therefore, after obtaining an experimental data file containing measurements of voltage, amperage, and temperature on a second-by-second basis, post-processing using MATLAB (MathWorks, Inc., Natick, Massachusetts, U.S.A.) calculated changes to battery capacity and its SOC for model calibration. For example, a sample SOC calculation of the LMN battery (2.0 A h) during a 0.5 C test is useful to understand the Peukert analysis methodology:

a) $C^0 = 2$ (rated nominal capacity)
b) $I_1 = 2\,\text{A h} \times 0.5\,\text{hr}^{-1} = 1$ A (amperage draw corresponding to 0.5 C test)
c) $\text{SOC}_0 = 100\%$ (starts fully charged)
d) Initial capacity: $Cap_0 = \text{SOC}_0 \times C^0 = 2.0$ A h
e) Time step of 60 s: $\Delta t = 0.01667$ h
f) Experimental capacity lost over time step: $Cap_{lost} = I_1 \times \Delta t = 1$ A × 1.667E-2 hr = 1.667E-2 A h
g) Capacity after time step: $Cap_1 = Cap_0 - Cap_{lost} = 2.0$ A h − 1.667E-2 A h = 1.983 A h
h) SOC after time step: $\text{SOC} = Cap_1/Cap_0 = 99.16\%$

However, this effort uses a new definition and calculation for steps (d) and (f), respectively. Specifically, a replacement of the initial capacity with $C_r^0$ and that the capacity lost over the time step now employs both the amperage draw and thermistor measurement. Hence, step (f) is now dependent on γ, $\alpha$, and $\beta$ via Eqn. (5).

Subsequently, calibration of the model parameters utilized the Matlab function *fmincon* employing the interior-point option that minimized a nonlinear Least-Squares Curve-fit (LSQ) comparison between model predicted final DOD and the experimental result of 100%. As a starting point for calibration, the researchers assumed that the battery holds the rated capacity; therefore, the initial values of $C_r^0$ were set equal to the manufacturers' Ah ratings. The logic of capacity offset dictates that $\alpha$ be near or just above one; hence, the initial $\alpha$ was set equal to one. The $\beta$ term dictates temperature behavior and the initial guess here is set equal to zero in order to predict a perfect battery independent of temperature effects. From this information, γ can be initially estimated from each experiment and an average γ was used as the starting point for calibration.

## 3. Results and discussion

It is imperative to the user of batteries in a mobile application that they trust the instrumentation's prediction of “empty” to alleviate range anxiety. Therefore, modeling the rate of capacity drain with respect to load and temperature is a crucial facet when simulating Li-ion batteries. Here, Table 2 provides calibrated model parameters as a function of the five distinct battery chemistries tested. In this table, a row containing

**Table 2**
Model parameters of tested Li-ion batteries after calibration to experimental data.

| Battery Name | Nominal Capacity [Ah] | Cathode Chemical Formula | $C_r^0$ multiplier | γ | $\alpha$ | $\beta$ | LSQ |
|---|---|---|---|---|---|---|---|
| LCO | 2.8 | $LiCoO_2$ | 100.13% | 0.8969 | 1.4374 | 0.0209 | 0.3008 |
| | | | 100.55% | 0.9844 | 1.2118 | 1.3543 | 0.0544 |
| LCO retest | 2.8 | $LiCoO_2$ | 112.39% | 0.9891 | 1.5143 | 0.0000 | 0.6657 |
| | | | 100.62% | 1.0016 | 1.2423 | 0.0037 | 0.0655 |
| NCA | 3.1 | $LiCoNiAlO_2$ | 100.58% | 1.1025 | 1.0456 | 0.7617 | 0.0523 |
| | | | 100.64% | 1.1019 | 1.0469 | 0.6826 | 0.0498 |
| NMC1 | 2.6 | $LiNiMnCoO_2$ | 101.10% | 0.9891 | 1.0530 | 2.6969 | 0.0991 |
| NMC2 | 2.2 | $LiNiMnCoO_2$ | 100.16% | 0.9161 | 1.6806 | 0.0133 | 0.3685 |
| | | | 100.43% | 1.0127 | 1.1868 | 1.7464 | 0.0351 |
| NMC2 retest | 2.2 | $LiNiMnCoO_2$ | 85.59% | 0.9506 | 1.5857 | 0.0030 | 0.4208 |
| | | | 101.27% | 1.0323 | 1.2822 | 0.0424 | 0.1367 |
| LMN | 2.0 | $LiMnNiO_2$ | 100.63% | 1.0079 | 1.1664 | 1.8943 | 0.2102 |
| | | | 100.40% | 1.0108 | 1.0919 | 0.7676 | 0.0265 |
| LFP1 | 1.1 | $LiFePO_4$ | 100.04% | 1.0193 | 1.0093 | 0.0081 | 0.0091 |
| LFP2 | 1.5 | $LiFePO_4$ | 105.09% | 1.0726 | 1.0232 | 0.0030 | 0.0313 |
| LFP3 | 2.5 | $LiFePO_4$ | 101.35% | 1.0411 | 1.0287 | 0.2483 | 0.0063 |

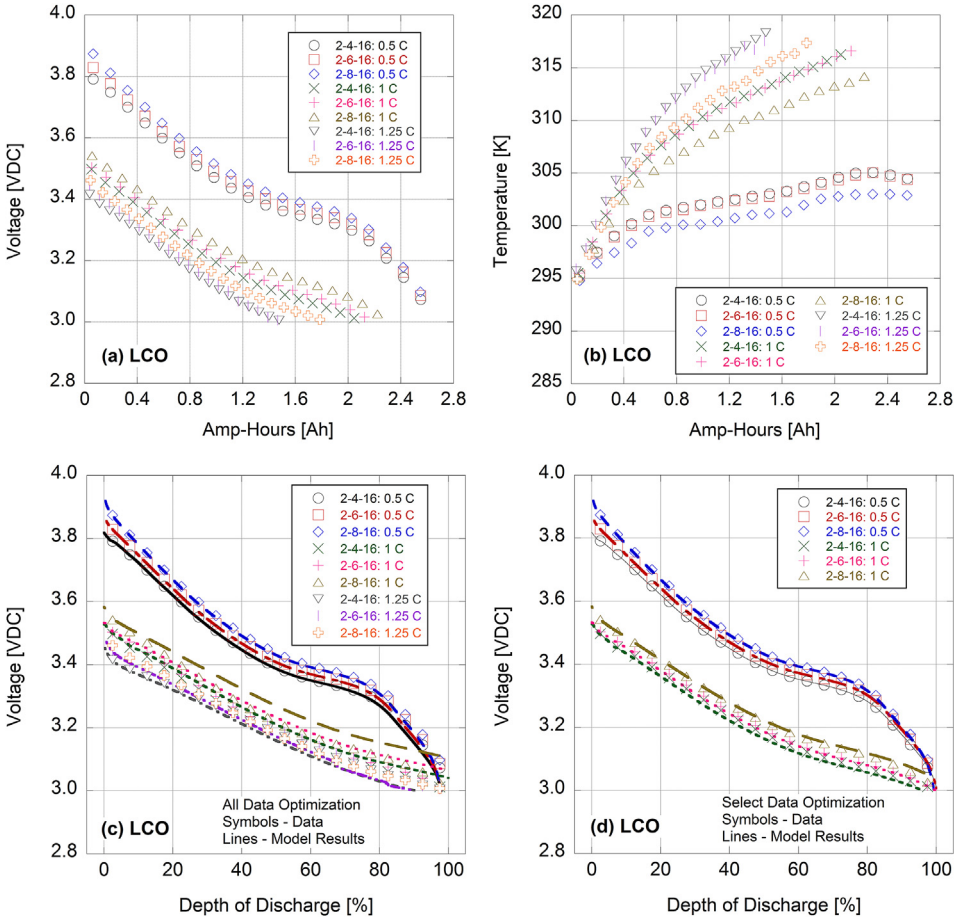


**Fig. 3.** Initial testing of LCO battery providing experimental (a) voltage and (b) temperature versus amp-hour rating along with model results as a function of depth of discharge for (c) all runs and (d) select data points. Note: the legend indicates the date (e.g., month-day-year) and C-Rating of each test.

two lines means that certain experimental data points were omitted in the second row based on discussed observations. Of note, in order to provide a truer comparison between the model and experiments, the figures presented provide the results as a function of an experimental normalized DOD; i.e., the final DOD scales all experimental results so that they end at 100%.

In general, layered compounds are isostructural to the layered framework with the $O^{2-}$ packed in a cubic and the transition metal element (e.g., Co, Ni) and $Li^{+}$ occupying the octahedral sites of an "O3-type" structure with a stacking sequence ABCABC. For layered compounds, e.g., the LCO battery, testing demonstrated in Fig. 3a that this battery is highly dependent on the C-rating. As discussed by Zhang et al. for LCO batteries the movement of a significant number of lithium ions relatively quick prevents a phase transition and equilibrium between ordered and disordered lithium ions in the $CoO_2$ crystal [40]. Hence, one does not see the typical lithium plateau under high discharge rates. Moreover, with respect to temperature, the LCO battery was found to generate a respectively significant amount of heat in Fig. 3b. Nitta et al. point out that this characteristic thermal instability is due to the released oxygen reacting with the organic materials during cycling. The self-heating due to the ion diffusion causes oxygen to react exothermically with the cathodic and electrolytic compounds [41]. Then, this action releases more heat into the system, which is the basis of the thermal run away and potential combustion effects mentioned prior. Other work by Doughty and Roth show that most species decompose and introduce self-heating oxygen into the system. However, the LCO chemistry does this at a lower temperature and at a faster rate than others, while the stable LFP seems to maintain its oxygen in its non-reactive state [42]. The reason for this perceived instability follows delithiation of the LCO framework during the phase change. Furthermore, with $Li_xCoO_2$ ($x < 0.5$) a secondary exothermic peak is reached as the structure abandons a layered state and forms a more spinel lattice with the cubic symmetry (space group *Fd3m*). As in other phase change reactions, this indicates a unique outlet of thermal energy [43]. Overall, understanding the implications of thermal instability is important in determining the limitations of this compound along with its relative temperature functionality in Eqn. (5).

Specifically, the choice of the multiplication factor for Eqn. (5) stemmed from the fact that both the current and temperature influence capacity offset in a similar manner. As current increases and temperature decreases, capacity offset grows; therefore, when temperature increases, battery capacity grows. Under high currents (i.e., the C-rating) during discharge, LCO batteries do not undergo a phase transition resulting in a relatively quick loss of capacity [44]; however, the temperature grows relatively rapidly because of its characteristic thermal instability. This rapid rise of temperature could lead to entropy changes that originate from a structural transformation in the anode and phase transition of the LCO cathode [45], which help to retain/recover the cell's capacity to some extent.

Initial optimization of all tests in Fig. 3c resulted in a relatively high LSQ owing to the fact that the 1.25C tests provided less than 50% of the rated capacity. Considering that possibility the battery was tested at too high a C-rating (although within the manufacturer's specification), these data were removed from the optimization resulting in a better fit of model and data via Fig. 3d with the corresponding parameters given in the second row of Table 2. Furthermore, to ensure that the battery was tested properly, it was retested a number of months later after the first LFP battery (shown with high testing accuracy later in this section).

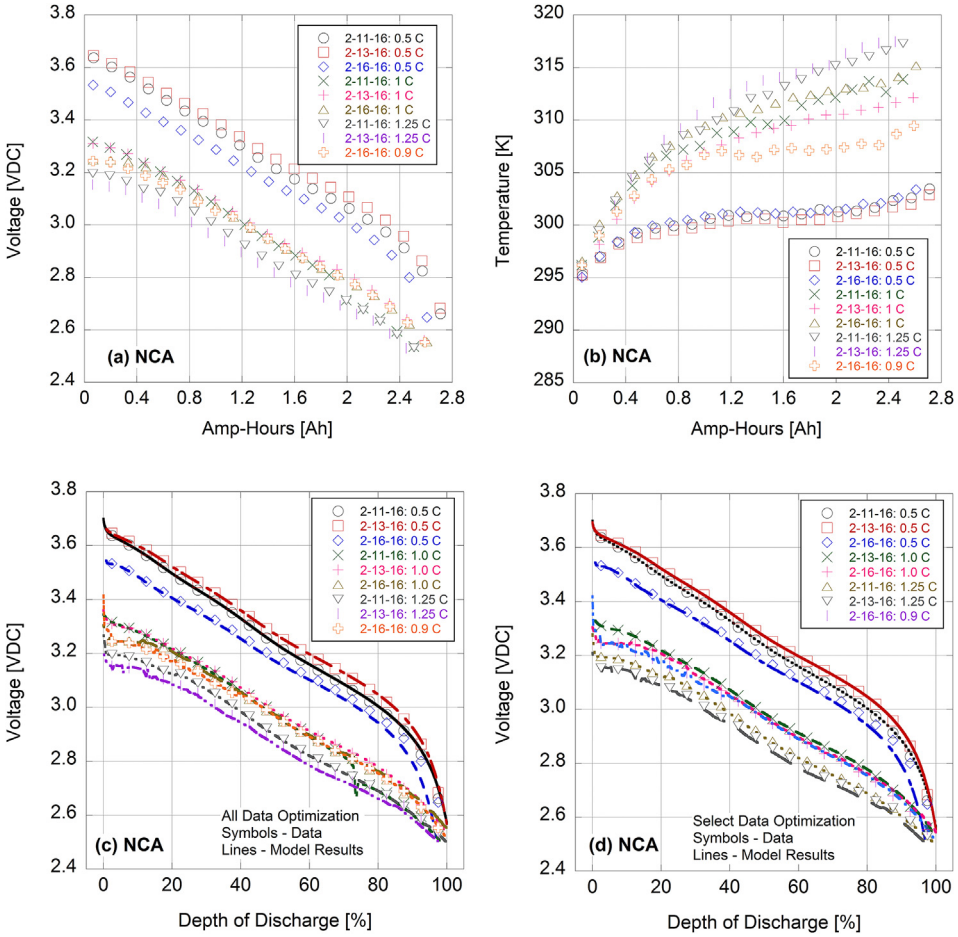


**Fig. 4.** Testing of NCA battery providing experimental (a) voltage and (b) temperature versus amp-hour rating along with model results as a function of depth of discharge for (c) all runs and (d) select data points. Note: the legend indicates the date (e.g., month-day-year) and C-Rating of each test.

Interestingly, the same issues that arose at 1.25C were found with the later tests (presented in the Supplemental Information). Performing an optimization over just the retests found a high degree of error for the model as demonstrated by the corresponding LSQ in Table 2. Removing the 1.25C retests and optimizing over all 0.5C and 1C tests (except for an assumed outlier) was able to model these data relatively accurately via second row of LCO retest in Table 2.

Overall, with increasing C-rate the LCO cells experienced a high overpotential in not only the electrode, but the electrolyte, which could cause the discrepancy. In addition, the retested cells were aged under both cycling and storage conditions; hence, this discrepancy may imply the adverse effects of battery aging and degradation. Of interest, the $\beta$ parameter changed significantly between the first optimization and the second. Looking at the raw data, the battery heated up relatively the same amount between these distinct tests (est. 20 K vs. 15 K at 1C for initial and retest, respectively), but optimization placed more of an emphasis on the $\alpha$ parameter. A relative conclusion as to $\alpha$ versus $\beta$ dependency for this battery will be revisited later in this section.

In Fig. 4, testing of the NCA battery demonstrated a higher level of repeatability than the LCO battery. Investigating individual experiments, only the 2-11-16 test employing a 1C discharge rate demonstrated an erroneous step voltage change around 2 A h in Fig. 4a; hence, representative optimized model results are shown including it in Fig. 4c and removing it in Fig. 4d (with corresponding rows in Table 2). Moreover, a 0.9C test was run instead of a final 1.25C test by oversight with its results kept in both optimization efforts. The results of the tests point towards the need to understand the geometry and underlying chemical behavior involved in the NCA cells. Overall, the literature underlines the inherent stability found in these species. Current technologies employ aluminum-doping of a base $LiNiCoO_2$ cathode and this additional presence of 0–5% Al suppresses the cell impedance rise associated with the surface reactions between the cathode and electrolyte without sacrificing capacity [46]. This benefit is attributed to the shape of the particles on the surface of the cathode. It makes sense that rounded particles with a low surface-area-to-volume ratio help limit the available area for the electrolyte to interact with, for a given volume. The effect of Al-doping forms a desirable “powder morphology”; i.e., tightly packed, spherical particles that are well suited to limit the solid-electrolyte-interface (SEI) surface area resulting in a stabilized cell [46]. Furthermore, the consistency of the discharge curves shown in Fig. 4 and the literature's stated stability both indicate high cycle ability; i.e., a low loss of capacity over many cycles. For example, Zhang and Wang performed long term cycling ($>$ 5000) using the NCA cathode and showed capacity fade on par with 1000 cycles of other chemistries [47]. They attribute this to the fact that in most batteries, capacity fade is due to a decrease in the number of intercalation sites on the cathode. This is a characteristic that the NCA does not demonstrate, resulting in low capacity fade.

However, while the NCA species has many desirable characteristics if properly used, the effects of elevated temperatures (Fig. 4b) are a drawback. In particular, Huang et al. compared the thermal stability of many common cathodes and state that at high SOCs, the low Li concentrated NCA starts to decompose around 200 °C resulting in a highly exothermic event with the potential for a dangerous thermal runaway [48]. In addition, transition metal ions (e.g., $Mn^{2+}$, $Co^{2+}$) tend to (particularly at elevated temperatures) dissolve into the electrolyte,

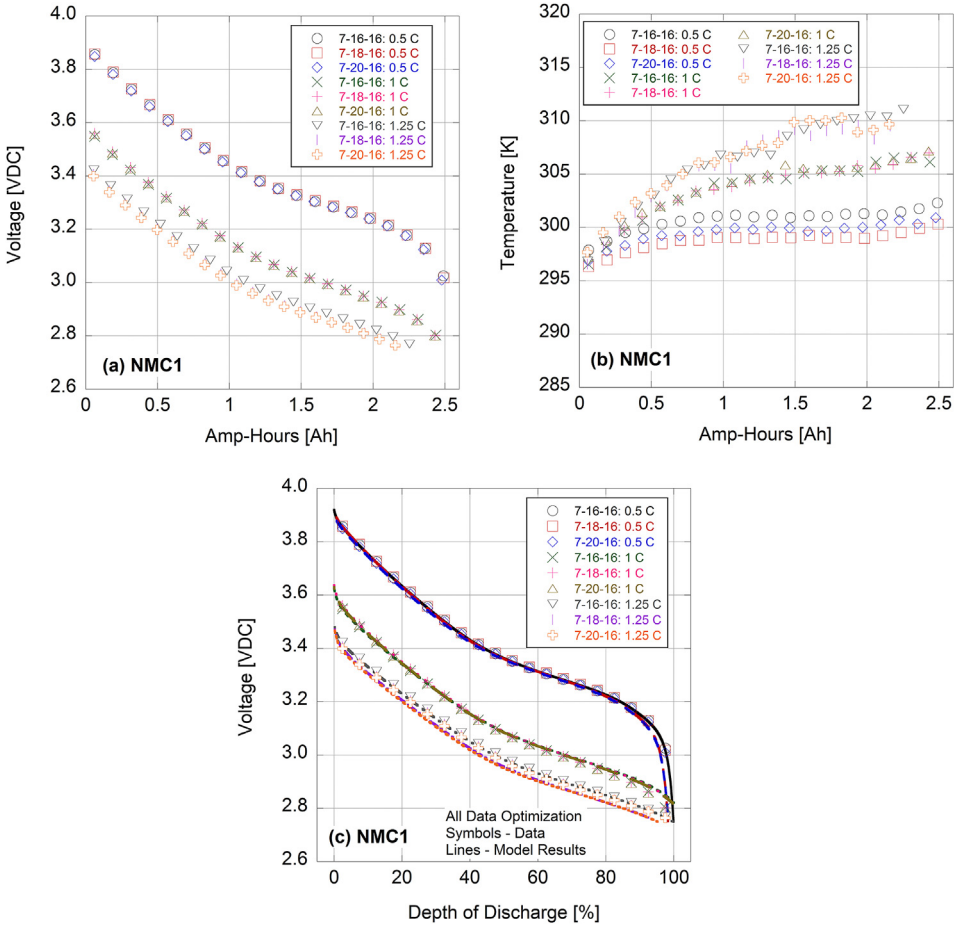


**Fig. 5.** Testing of NMC1 battery providing experimental (a) voltage and (b) temperature versus amp-hour rating along with model results as a function of depth of discharge for (c) all runs. Note: the legend indicates the date (e.g., month-day-year) and C-Rating of each test.

induce oxygen release, and increase cell resistance, which further elevates battery temperature and degrades its capacity. Moreover, the capacity fade of NCA can be severe at an elevated temperature due to electrochemical cycling-induced material fatigue and failures, such as cracking at NCA grain boundaries [49].

Testing the first NMC battery found an extremely repeatable set of data across all tests in Fig. 5. As a result, optimization performed over all runs resulted in relatively good model matching. The characteristics of the curves indicate a lower temperature rise as compared to the similarly constructed LCO cells. Incorporating Ni and Mn in place of Co is a common technique as both are cheaper than Co with Mn being significantly less hazardous. In comparison, Gotcu et al. experimentally determined the heat capacity and thermal diffusivity of NMC cathodes and found it to be higher than LCO, subsequently resulting in an increased heat transfer and storage [50]. Analogous to Furushima et al. [51], they were able to show that this increase in thermal conductivity is more pronounced in delithiated samples, corresponding to a fully charged battery where thermal runaway is of concern. All of these aspects lead to a reduced temperature rise for NMC batteries and higher onset temperature for self-heating.

In addition to the more desirable thermal attributes associated with substituting these other transition metals in for Co, there exist some drawbacks. One major problem is to determine the cation mixing between nickel and lithium ion because their radii are close, $Ni^{2+}$ (0.69 Å) vs. $Li^{+}$ (0.76 Å). Specific capacity can be diminished by the presence of Ni atoms in the Li-ion layer, made possible due to their relatively similar sizes. In addition, the lower electronegativity of Mn decreases the overall voltage potential as seen in Fig. 5. Since NMC batteries form a framework similar to $CoO_2$, the prior discussion involving the lack of discharge plateauing demonstrated by Zhang et al. is valid here. Moreover, as indicated by Li et al. the transition between a layered $Li_2MnO_3$ lattice and a $MnO_2$-like phase under higher charging and discharging rates might be rate limited (i.e., slow kinetics) [52]. Overall, the drawbacks associated with introducing Ni or Mn alone appear to be offset by each other's benefits while thermal stability increases as more Co atoms are replaced with Ni and Mn atoms [53].

Interestingly, analyzing the second NMC battery from the same manufacturer found a drastically different outcome as a function of current in Fig. 6; whereas, it appears that the temperature rise was fairly consistent between the two batteries. This battery could not handle 1C experiments with a loss in capacity of over 50% in one case. Moreover, the 0.5C test on 8-24-16 was found to have a sudden voltage drop for no reason. Similar to the LCO trials, a second set of data was taken for this battery later to see if better results could be generated. This later test (provided in Supplementary Information) demonstrated even bigger swings in repeatability with the 1C tests dropping into the 30% capacity range. Calibrating across all data found a significantly large error since the data had substantial variability. Removing the apparently erroneous trials helped to increase the model accuracy, although not to the point of the first NMC battery tested. Analogous to the LCO testing, this reduced repeatability resulted in a greater $\alpha$ calibrated parameter with the influence on $\beta$ dropping. This makes sense after reviewing the NCA and NMC1 tests that had $\alpha$ parameters closer to unity. It is theorized here that those batteries were manufactured with tighter tolerances; hence, they become more repeatable when testing as a function of current. Moreover, via a thermal analysis of NMC as published recently, the battery self-heating rate closely relates to both SOC and State of Health (SOH) that influences the reaction kinetics

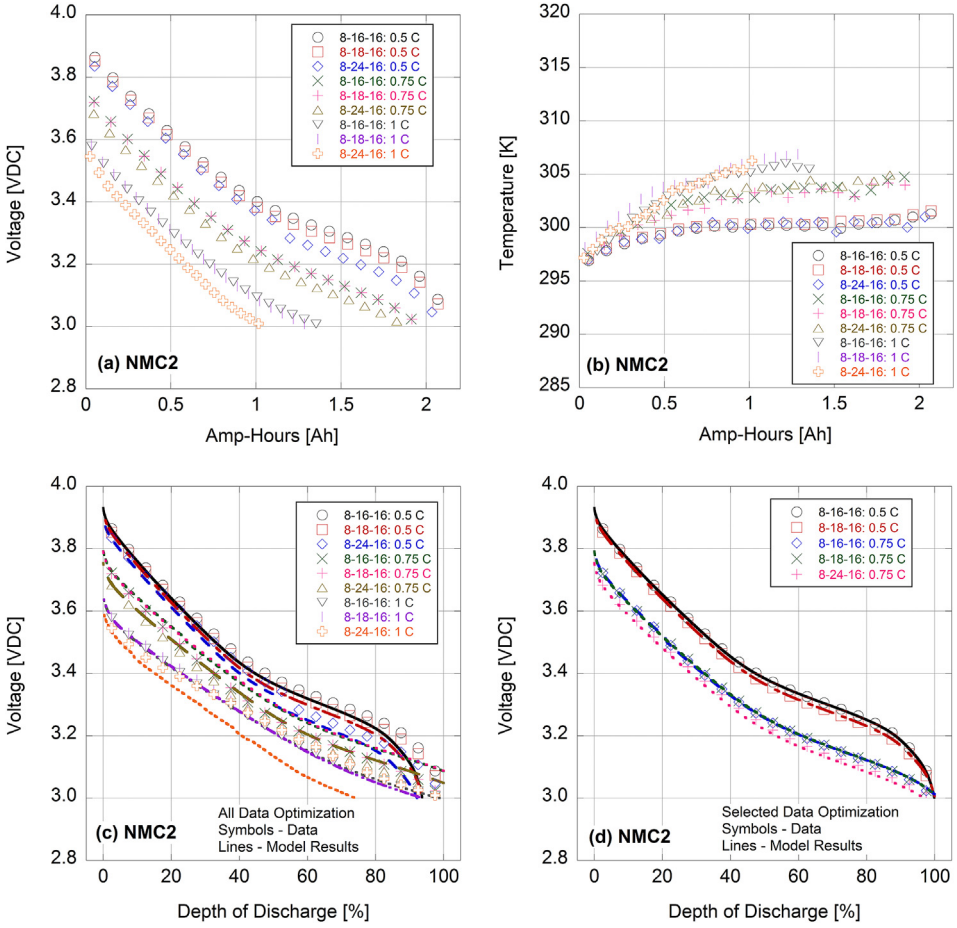


**Fig. 6.** Testing of second NMC battery providing experimental (a) voltage and (b) temperature versus amp-hour rating along with model results as a function of depth of discharge for (c) all runs and (d) select data points. Note: the legend indicates the date (e.g., month-day-year) and C-Rating of each test.

[54]. Therefore, the changing temperature with discharge current begins to play a larger role in modifying the capacity of these batteries. More importantly, it is essential and critical to monitoring and tracking the SOH of these batteries. Although the SOH may not directly correspond to a particular physical parameter, many researchers use Electrochemical Impedance Spectroscopy (EIS) to investigate the battery cell's degradation occurring not only in the electrodes but also in the electrolyte. Whereas, for the LCO and NMC2 batteries, the variance in day-to-day tests with current are reflected in a greater $\alpha$ that significantly overshadows the effects of temperature. This illustrates the need to test all batteries to determine their respective $\alpha$ and $\beta$ values before implementing in an electric vehicle instead of relying on a literature source. Furthermore, taking additional data can provide parameters that are more accurate by helping to reduce standard deviations in the tests.

Fig. 7a illustrates that the LMN battery had two repeatable days with one day demonstrating a reduced capacity. Moreover, in Fig. 7b the battery had a significant reduction in heat generation. The overall optimized results in Fig. 7c are skewed by the one dissimilar day and removing these data ended in generating a low LSQ error for the model in Fig. 7d. Overall, similar behavior to the NMC cathode is shown due to LMN's analogous chemistry. Specifically, the presence of Ni and Mn atoms increase thermal conductivity and specific heat properties, subsequently minimizing temperature rise. However, the absence of Co atoms in the lattice is a significant aspect as Co allows a more spinel shape to form. It is correct that $LiMn_2O_4$ forms a truer spinel, but the addition of Ni atoms restrain the Mn ions to the $^{+4}$ oxidation state and avoid unwanted lattice distortion and energy loss [55]. Spinel structures mark a definitive difference in this species as it allows for three-dimensional movement of Li-ions. Although difficult to tell from the data, the spinel lattice theoretically produces a greater specific capacity because it avoids the tendency of ions to skip empty sites, which is more common in the layered structures. This aspect combined with its thermal stability makes LMN more desirable in certain applications.

Generally, olivine compounds (e.g., LFP batteries) possess a distorted hexagonal close-packed structure where Li and Fe ions located in half of the octahedral sites and P occupying one-eighth of the tetrahedral sites, as shown in Fig. 1. The testing of the LFP batteries found consistent results between all batteries in Fig. 8 and in the Supplemental Information. Except for an unknown dip in voltage for one test at 0.5C with LFP2 and the 1C and 1.25C tests with LFP3, all LFP voltage, temperature, and model profiles were similar. Moreover, this battery chemistry heated up the least amount. Hence, both $\alpha$ and $\beta$ parameters were low since repeatability was high and temperature did not significantly influence the findings. This is because LFP batteries are less affected by the discharging rate because of their enhanced Li ion insertion and extraction along with improved electrode kinetics [6].

Due to the consistent behavior of the olivine species, the researchers observed an interesting phenomenon. The strategy to normalize the load for each cell (i.e., using C-ratings) should produce similar loading behavior regardless of cell size. However, upon initial loading of the highest power test, each of the different capacity LFP batteries studied displayed dissimilar voltage drops. This variance demonstrates distinctive reactionary stresses that develop in the SEI that are not straightforward. As mentioned before, significant effort in understanding the effects of different internal resistances is under current pursuit. Of interest here is the SEI resistance that can suffer from crystallization and other side reactions or physical failures, such as

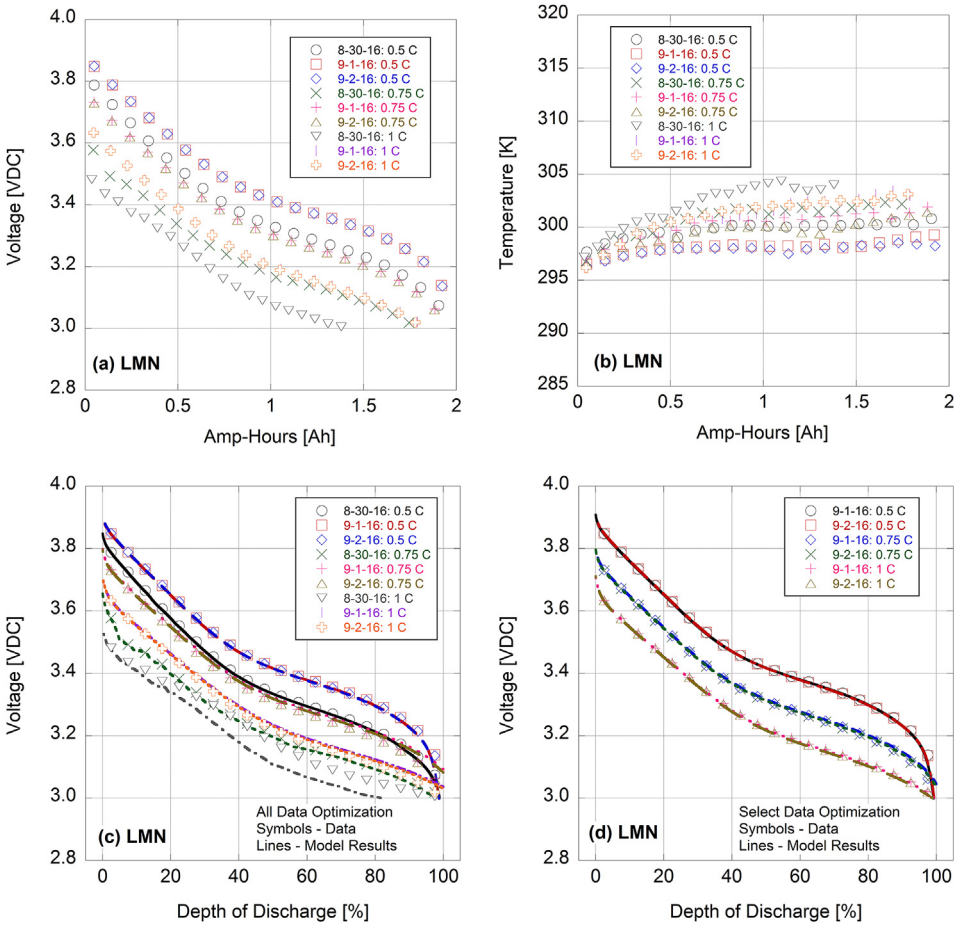


**Fig. 7.** Testing of LMN battery providing experimental (a) voltage and (b) temperature versus amp-hour rating along with model results as a function of depth of discharge for (c) all runs and (d) select data points. Note: the legend indicates the date (e.g., month-day-year) and C-Rating of each test.

"drying out" or gas generation and dissipation [56]. The inconsistencies in these data may reflect the initial use of the manufacturer supplied "C-rating" in the experimental set up; however, this aspect is included in the model. Hence, further research is necessary to understand initial loading behavior and its relationship with capacity and size, and the improved model seems to be a useful tool in this pursuit.

Overall, this attempt to remove the temperature factor from the standard Peukert coefficient ($\alpha$) and instead correlate it to the phenomena of ionic diffusivity and electron resistance in both the cathodic structure and electrolyte solution encountered limited success. Those batteries tested with some repeatability (NCA, LMN, NMC1, and LFP) demonstrated functional $\beta$ dependencies. While the battery that heated up the least (LFP) had the lowest $\beta$ term, there was not a direct correlation between $\beta$ and the other chemistries (i.e., temperature rise: NCA > NMC1 > LMN, but $\beta$: NMC1 > LMN > NCA). For the other batteries (LCO and NMC2), the inability to repeat data points skewed the results towards the $\alpha$ term, subsequently removing the functional temperature dependency. Moving forward, taking more tests to remove the standard deviation in experimental data should help determine more accurate model parameters. Moreover, correlating the repeatability to (assumed) manufacturing tolerances would help place these findings in a better light. Furthermore, enhanced modeling techniques using multi-scale computational methods can help understand the microstructure evolvement and (de)lithiation induced phase transformation during the (de)intercalation processes [57] helping to construct better batteries while translating their results to more simplistic models, such as the one employed here. Finally, by scaling all experimental data to end at 100% DOD, this results in relatively good agreement between data and the model. This is because the model was designed to end at 100% DOD through its use of an absolute capacity that helps normalize all distinct discharging scenarios. From an on-board vehicle perspective, now a voltage map as a function of discharge rate and DOD can be employed along with the enhanced Peukert model in order to more accurately predict the range left in the batteries.

## 4. Conclusions

A main obstacle in further adaptation of the current electric vehicle market is range anxiety, but mitigation of this condition can occur through proper battery modeling. Previous research has elucidated the efficacy of an enhanced Peukert model of battery discharge that improves on older, less accurate state-of-charge prediction techniques by incorporating temperature, chemistry-specific parameters, and a redefinition of absolute capacity. This research successfully applied the enhanced model to LCO, NCA, NMC, LMN, and LFP chemistries and validated the applicability for most current EV battery chemistries. The behavior of the model curves for many of the species follows patterns consistent with the current literature. The exothermic and thermally unstable LCO species resulted in a high temperature parameter, $\beta$, which makes sense for a thermally sensitive reaction. Contrarily, the moderately scaled $\beta$ term found for the NCA indicate the known stability of these types and in proven longevity. Similarly, the low parameters that were obtained that are associated with elevated current, namely $\alpha$, were indicative of the low capacity offset common in the LFP varieties. The layered varieties represented by NMC and LMN show the most variation as they have the most stoichiometric varieties and kinetic phases, but tend to fall in the middle regarding stability and offset. This variation is due to different manufacturers' chemistry, but once the

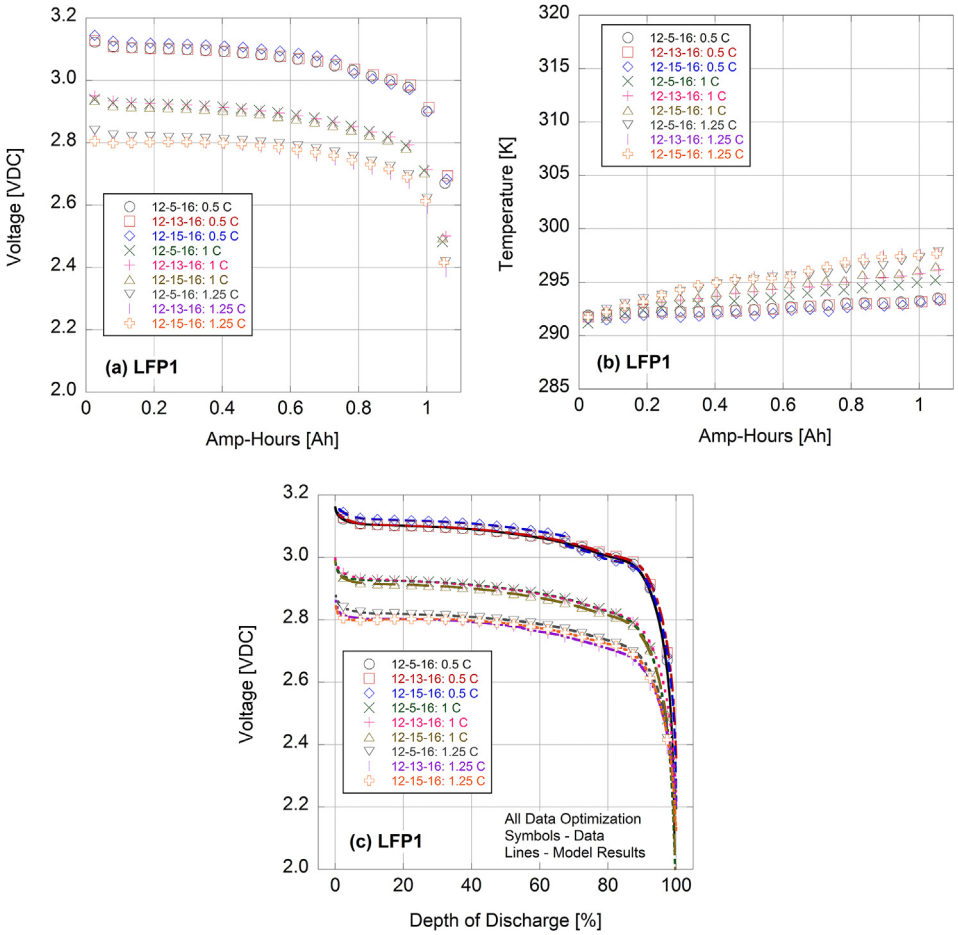


**Fig. 8.** Testing of LFP1 battery providing experimental (a) voltage and (b) temperature versus amp-hour rating along with model results as a function of depth of discharge for (c) all runs. Note: the legend indicates the date (e.g., month-day-year) and C-Rating of each test.

parameters for a particular species are known, they may be used as a basis for modeling. The research outlined here also shows the inherent difficulty in modeling chemical reactions with so many interdependent variables. While some of the data were disregarded due to obvious day-to-day experimental issues, many tests were performed and the overall ability of the improved model to capture the known behaviors of the common EV batteries types proves its utility in future efforts.

The results show that engineers can choose an appropriate chemistry based on desired complexity and performance by comparing model parameters. Manufacturer-supplied information, such as voltage ranges, nominal capacities, and maximum loads are useful, but the information gleaned from the improved model provides more insight and leads to a better design. A short-term achievement of this work will be to develop a "fuel gauge" for a vehicle using one of the exact chemistries tested. Using parameters obtained through the model, $C_r^0$, $\alpha$, $\beta$, and $\gamma$, a BMS can be merely programmed to obtain a better understanding of remaining energy stored while the vehicle is driven. When more types of cells are tested using the same techniques, a resource can be developed for all future battery pack designs to utilize. This is an underlying strength of the current field of research as many chemistries are being studied by an even larger number of researchers. Insights into the underlying chemistry and new ideas concerning modeling are abundant, which will lead to safe and more controllable battery packs.

## Acknowledgements

Dr. L. Liu would like to thank the financial assistance from Kansas NASA EPSCoR program and Ningxia Colleges and Universities Science and Technology Research Project NGY2017160. Moreover, the authors wish to thank Marc Venis and Vencon Technologies Inc. for their assistance in the recalibration process prior to data collection.

## Appendix A. Supplementary data

Supplementary data related to this article can be found at http://dx.doi.org/10.1016/j.jpowsour.2018.06.066.

## References

[1] U.S. Department of Energy, Alterative Fuels Data Center, Energy Efficiency & Renewable Energy, (2018) https://www.afdc.energy.gov/fuels/prices.html , Accessed date: 4 February 2018.
[2] J. Neubauer, E. Wood, The impact of range anxiety and home, workplace, and public charging infrastructure on simulated battery electric vehicle lifetime utility, J. Power Sources 257 (2014) 12–20.
[3] W. Peukert, Über die Abhängigkeit der Kapazität von der Entladestromstärke bei Bleiakkumulatoren, Elektrotech. Z. 20 (1897) 20–21.
[4] N. Omar, P. Bossche, T. Coosemans, J. Mierlo, Peukert revisited—critical appraisal and need for modification for lithium-ion batteries, Energies 6 (2013) 5625.
[5] S.S. Zhang, K. Xu, T.R. Jow, Charge and discharge characteristics of a commercial $LiCoO_2$-based 18650 Li-ion battery, J. Power Sources 160 (2006) 1403–1409.
[6] J. Wang, X. Sun, Understanding and recent development of carbon coating on $LiFePO_4$ cathode materials for lithium-ion batteries, Energy Environ. Sci. 5 (2012) 5163–5185.
[7] W. Zhang, Y. Zeng, C. Xu, N. Xiao, Y. Gao, L.-J. Li, X. Chen, H.H. Hng, Q. Yan, A facile approach to nanoarchitectured three-dimensional graphene-based Li–Mn–O composite as high-power cathodes for Li-ion batteries, Beilstein J. Nanotechnol. 3 (2012) 513–523.
[8] J.W. Fergus, Recent developments in cathode materials for lithium ion batteries, J. Power Sources 195 (2010) 939–954.
[9] A. Hausmann, C. Depcik, Expanding the Peukert equation for battery capacity modeling through inclusion of a temperature dependency, J. Power Sources 235 (2013) 148–158.

[10] S. Peck, M. Pierce, Development of a temperature-dependent Li-ion battery thermal model, SAE Paper 2012-01-0117, 2012.
[11] X. Liu, J. Wu, C. Zhang, Z. Chen, A method for state of energy estimation of lithium-ion batteries at dynamic currents and temperatures, J. Power Sources 270 (2014) 151–157.
[12] Y. Liu, T. Zhao, W. Ju, S. Shi, Materials discovery and design using machine learning, Journal of Materiomics 3 (2017) 159–177.
[13] H. He, R. Xiong, H. Guo, S. Li, Comparison study on the battery models used for the energy management of batteries in electric vehicles, Energy Convers. Manag. 64 (2012) 113–121.
[14] V.H. Johnson, Battery performance models in ADVISOR, J. Power Sources 110 (2002) 321–329.
[15] Z. Jiucai, C. Song, H. Sharif, M. Alahmad, An enhanced circuit-based model for single-cell battery, Applied Power Electronics Conference and Exposition (APEC), 2010 Twenty-Fifth Annual IEEE, 2010, pp. 672–675.
[16] D. Doerffel, S.A. Sharkh, A critical review of using the Peukert equation for determining the remaining capacity of lead-acid and lithium-ion batteries, J. Power Sources 155 (2006) 395–400.
[17] M. Doyle, J. Newman, J. Reimers, A quick method of measuring the capacity versus discharge rate for a dual lithium-ion insertion cell undergoing cycling, J. Power Sources 52 (1994) 211–216.
[18] J. Wang, P. Liu, J. Hicks-Garner, E. Sherman, S. Soukiazian, M. Verbrugge, H. Tataria, J. Musser, P. Finamore, Cycle-life model for graphite-$LiFePO_4$ cells, J. Power Sources 196 (2011) 3942–3948.
[19] S.H. Oh, J.C. Cavendish, Transients of monolithic catalytic converters: response to step changes in feedstream temperature as related to controlling automobile emissions, Ind. Eng. Chem. Res. 21 (1982) 29–37.
[20] V.A. Streltsov, E.L. Belokoneva, V.G. Tsirelson, N.K. Hansen, Multipole analysis of the electron density in triphylite, $LiFePO_4$, using X-ray diffraction data, Acta Crystallogr. B 49 (1993) 147–153.
[21] Z. Lu, D.D. MacNeil, J.R. Dahn, Layered Li $[Ni_xCo_{1-2x}Mn_x]O_2$ cathode materials for lithium-ion batteries, Electrochem. Solid State Lett. 4 (2001) A200–A203.
[22] General Motors Corporation, Chevrolet Volt Battery System, (2016) 2016 https://media.gm.com/content/dam/Media/microsites/product/Volt_2016/doc/VOLT_BATTERY.pdf , Accessed date: 15 May 2018.
[23] E. Timofeeva, The Spectrum of EV Battery Chemistries, (2017) http://www.influitenergy.com/the-spectrum-of-ev-battery-chemistries/ , Accessed date: 15 May 2018.
[24] K.I. Ozoemena, S. Chen, Nanomaterials in Advanced Batteries and Supercapacitors, Springer International, Switzerland, 2016.
[25] Qnovo Incorporated, Inside the Battery of a Nissan Leaf, (2015) https://qnovo.com/inside-the-battery-of-a-nissan-leaf/ , Accessed date: 15 May 2018.
[26] M. Dubarry, C. Truchot, A. Devie, B.Y. Liaw, K. Gering, S. Sazhin, D. Jamison, C. Michelbacher, Evaluation of commercial lithium-ion cells based on composite positive electrode for plug-in hybrid electric vehicle (PHEV) applications: IV. Over-discharge phenomena, J. Electrochem. Soc. 162 (2015) A1787–A1792.
[27] K. Fehrenbacher, Why Tesla's Grid Batteries will Use Two Different Chemistries, (2015) http://fortune.com/2015/05/18/tesla-grid-batteries-chemistry/ , Accessed date: 15 May 2018.
[28] M. Cheng, M. Tong, Development status and trend of electric vehicles in China, Chinese Journal of Electrical Engineering 3 (2017) 1–13.
[29] M. Choate, J. Meeth, C. Christianson, P. Collins, C. Depcik, A Swappable Battery Pack for Short-range Electric Vehicles, (2014) ASME IMECE2014–37080.
[30] U. von Sacken, E. Nodwell, A. Sundher, J.R. Dahn, Comparative thermal stability of carbon intercalation anodes and lithium metal anodes for rechargeable lithium batteries, J. Power Sources 54 (1995) 240–245.
[31] D. Andrea, Battery Management Systems for Large Lithium-ion Battery Packs, Artech House, Norwood, MA, 2010.
[32] X. Lin, J. Park, L. Liu, Y. Lee, A.M. Sastry, W. Lu, A comprehensive capacityfade model and analysis for Li-ion batteries, J. Electrochem. Soc. 160 (2013) A1701–A1710.
[33] C. Liu, L. Liu, Optimal design of Li-ion batteries through multi-physics modeling and multi-objective optimization, J. Electrochem. Soc. 164 (2017) E3254–E3264.
[34] L. Liu, J. Park, X. Lin, A.M. Sastry, W. Lu, A thermal-electrochemical model that gives spatial-dependent growth of solid electrolyte interphase in a Li-ion battery, J. Power Sources 268 (2014) 482–490.
[35] L. Liu, M. Zhu, Modeling of SEI layer growth and electrochemical impedance spectroscopy response using a thermal-electrochemical model of Li-ion batteries, ECS Transactions 61 (2014) 43–61.
[36] D. Linden, T.B. Reddy, Handbook of Batteries, third ed., McGraw-Hill, 2002.
[37] M. Ecker, J.B. Gerschler, J. Vogel, S. Käbitz, F. Hust, P. Dechent, D.U. Sauer, Development of a lifetime prediction model for lithium-ion batteries based on extended accelerated aging test data, J. Power Sources 215 (2012) 248–257.
[38] K. Smith, C.-Y. Wang, Power and thermal characterization of a lithium-ion battery pack for hybrid-electric vehicles, J. Power Sources 160 (2006) 662–673.
[39] D.H. Jeon, S.M. Baek, Thermal modeling of cylindrical lithium ion battery during discharge cycle, Energy Convers. Manag. 52 (2011) 2973–2981.
[40] Q. Zhang, Q. Guo, R.E. White, Semi-empirical modeling of charge and discharge profiles for a $LiCoO_2$ electrode, J. Power Sources 165 (2007) 427–435.
[41] N. Nitta, F. Wu, J.T. Lee, G. Yushin, Li-ion battery materials: present and future, Mater. Today 18 (2015) 252–264.
[42] D.H. Doughty, E.P. Roth, A general discussion of Li ion battery safety, The Electrochemical Society Interface 21 (2012) 37–44.
[43] Y. Baba, S. Okada, J.-i. Yamaki, Thermal stability of $Li_xCoO_2$ cathode for lithium ion battery, Solid State Ionics 148 (2002) 311–316.
[44] J. Cho, Y.J. Kim, B. Park, $LiCoO_2$ cathode material that does not show a phase transition from hexagonal to monoclinic phase, J. Electrochem. Soc. 148 (2001) A1110–A1115.
[45] S. Al Hallaj, R. Venkatachalapathy, J. Prakash, J.R. Selman, Entropy changes due to structural transformation in the graphite anode and phase change of the $LiCoO_2$ cathode, J. Electrochem. Soc. 147 (2000) 2432–2436.
[46] C.H. Chen, J. Liu, M.E. Stoll, G. Henriksen, D.R. Vissers, K. Amine, Aluminum-doped lithium nickel cobalt oxide electrodes for high-power lithium-ion batteries, J. Power Sources 128 (2004) 278–285.
[47] Y. Zhang, C.-Y. Wang, Cycle-life characterization of automotive lithium-ion batteries with $LiNiO_2$ cathode, J. Electrochem. Soc. 156 (2009) A527–A535.
[48] Y. Huang, Y.-C. Lin, D.M. Jenkins, N.A. Chernova, Y. Chung, B. Radhakrishnan, I.-H. Chu, J. Fang, Q. Wang, F. Omenya, S.P. Ong, M.S. Whittingham, Thermal stability and reactivity of cathode materials for Li-ion batteries, ACS Appl. Mater. Interfaces 8 (2016) 7013–7021.
[49] S. Watanabe, M. Kinoshita, T. Hosokawa, K. Morigaki, K. Nakura, Capacity fading of $LiAl_yNi_{1-x-y}Co_xO_2$ cathode for lithium-ion batteries during accelerated calendar and cycle life tests (effect of depth of discharge in charge–discharge cycling on the suppression of the micro-crack generation of $LiAl_yNi_{1-x-y}Co_xO_2$ particle), J. Power Sources 260 (2014) 50–56.
[50] P. Gotcu, W. Pfleging, P. Smyrek, H.J. Seifert, Thermal behaviour of $Li_xMeO_2$ (Me = Co or Ni + Mn + Co) cathode materials, Phys. Chem. Chem. Phys. 19 (2017) 11920–11930.
[51] Y. Furushima, C. Yanagisawa, T. Nakagawa, Y. Aoki, N. Muraki, Thermal stability and kinetics of delithiated $LiCoO_2$, J. Power Sources 196 (2011) 2260–2263.
[52] J. Li, R. Klöpsch, M.C. Stan, S. Nowak, M. Kunze, M. Winter, S. Passerini, Synthesis and electrochemical performance of the high voltage cathode material Li $[Li_{0.2}Mn_{0.56}Ni_{0.16}Co_{0.08}]O_2$ with improved rate capability, J. Power Sources 196 (2011) 4821–4825.
[53] D.D. MacNeil, Z. Lu, J.R. Dahn, Structure and electrochemistry of Li $[Ni_xCo_{1-2x}Mn_x]O_2$ $(0 \le x \le 1/2)$, J. Electrochem. Soc. 149 (2002) A1332–A1336.
[54] S. Hildebrand, A. Rheinfeld, A. Friesen, J. Haetge, F.M. Schappacher, A. Jossen, M. Winter, Thermal analysis of $LiNi_{0.4}Co_{0.2}Mn_{0.4}O_2$/mesocarbon microbeads cells and electrodes: state-of-charge and state-of-health influences on reaction kinetics, J. Electrochem. Soc. 165 (2018) A104–A117.
[55] C.M. Julien, A. Mauger, Review of 5-V electrodes for Li-ion batteries: status and trends, Ionics 19 (2013) 951–988.
[56] Z. Mao, M. Farkhondeh, M. Pritzker, M. Fowler, Z. Chen, Calendar aging and gas generation in commercial graphite/NMC-LMO lithium-ion pouch cell, J. Electrochem. Soc. 164 (2017) A3469–A3483.
[57] S.Q. Shi, J. Gao, Y. Liu, Y. Zhao, Q. Wu, W.W. Ju, C.Y. Ouyang, R.J. Xia, Multi-scale computation methods: their applications in lithium-ion battery research and development, Chin. Phys. B 25 (2016) 018212.